Effect of Micro and Bulk Solvation on the Mechanism of Nucleophilic Substitution at Sulfur in Disulfides

Joseph M. Hayes[†] and Steven M. Bachrach*

Department of Chemistry, Trinity University, 1 Trinity Place, San Antonio, Texas 78212

Received: May 21, 2003; In Final Form: July 28, 2003

Computational studies of the solution-phase mechanism of nucleophilic substitution at sulfur in disulfides with explicit water representation indicate that the pathway is dependent on the substituent on the sulfur under attack. B3LYP/6-31+G* optimizations for prototype thiolate-disulfide exchange reactions were performed including one to four explicit water molecules, followed by single-point free energy calculations with B3LYP/6-31+G* and the polarized continuum model (PCM). The solution-phase mechanism is the addition−elimination mechanism when the sulfur under attack bears a hydrogen, while the S_N2 mechanism is predicted when the sulfur substituent is a methyl group.

Introduction

Despite the importance of nucleophilic substitution reactions at heteroatoms such as sulfur, relatively little work has been done to determine features of the substitution mechanisms at these atoms. Nucleophilic substitution at sulfur has significant biological importance.[1] For example, the thiol-disulfide exchange plays an important role in the folding of proteins and is essential to the enzyme activities of flavin-containing dehydrogenases such as lipoamide dehydrogenases and glutathione reductase, which helps prevent the destruction of red blood cells.[2,3] Explication of the general mechanism for nucleophilic substitution at sulfur will help increase the understanding of the nature of these, and many more, biochemical processes. Solution-phase experimental studies have suggested that nucleophilic substitution at sulfur follows an S_N2 pathway (Figure 1d).[4−11] However, previous computational studies by our group have indicated that the mechanism is addition−elimination in the gas phase (Figure 1a).[12−15] Indeed, computations have shown that the intermediate is greatly stabilized when sulfur bears electronegative substituents; for the reactions of chloride with SCl_2 and $SOCl_2$, the minimum on the potential energy surface is the species where the nucleophile has added to the sulfur, i.e., SCl_3^- and $SOCl_3^-$, respectively.[16,17] Gas-phase flowing-afterglow MS studies identified these two hypercoordinate species and corroborate the depth of the computed wells.

Solvent can strongly affect the course of chemical reactions. For example, rates of S_N2 reactions in gas versus solution phase can vary by some 20 orders of magnitude.[18] Brauman's[19] extensive study of gas-phase S_N2 reactions have confirmed the double-well (see Figure 1c) potential energy surface (PES), in contrast to the familiar single-barrier PES in solution (see Figure 1d); the contrast is exquisitely demonstrated in Jorgensen's[20] molecular dynamics studies. Solvent can alter the potential energy surface shape, the position of the critical points, their relative energies, and the shape about the critical points.[21−23]

We are interested in the effect of solvent on the thiolate-disulfide exchange reaction. Preliminary computations to mimic the solution phase have indicated that addition−elimination may be the preferred pathway (Figure 1b).[15] The solution-phase calculations were performed using B3LYP/6-31+G* with the polarized continuum model (PCM) and indicate, consistent with the gas-phase computations, that for the thiolate-disulfide and thiolate-trisulfide exchange reactions where the sulfur under attack bears a hydrogen atom the substitution proceeds via an addition−elimination mechanism. However, when a methyl group is attached to the sulfur under attack, the S_N2 mechanism is predicted.

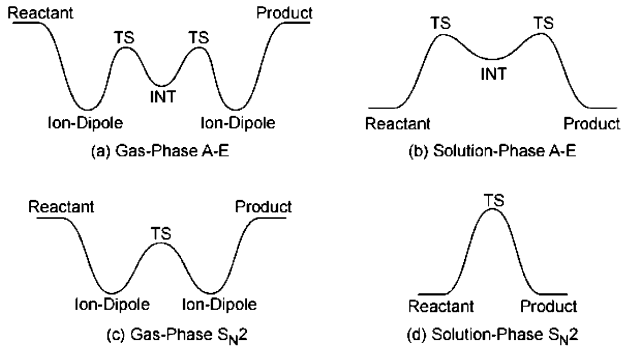

Figure 1. Schematic drawings of potential energy surfaces for nucleophilic substitution reactions.

Mohamed and Jensen[24] examined the role of water on the S_N2 reactions of chloride with primary, secondary, and tertiary alkyl chlorides. They examined the role of microsolvation by explicit consideration of up to four water molecules and then the role of the bulk solution by application of PCM to these microsolvated structures. We report here a similar approach of explicit consideration of the effects of one to four interacting water molecules, with and without PCM, on reactions 1−3. This report constitutes a more comprehensive study of solvation effects on the three disulfide exchange reactions we previously examined.[15]

$$HS^- + HSSH \rightarrow HSSH + HS^- \quad \text{(reaction 1)}$$

$$CH_3S^- + HSSCH_3 \rightarrow CH_3SSH + CH_3S^- \quad \text{(reaction 2)}$$

$$HS^- + CH_3SSH \rightarrow HSSCH_3 + HS^- \quad \text{(reaction 3)}$$

* Corresponding author. E-mail: sbachrach@trinity.edu.
[†] Current address: Anterio Consult & Research GmbH, Augustaanlage 26, 68165 Mannheim, Germany.

10.1021/jp035407f CCC: $25.00
Published on Web 08/30/2003

Computational Method

The three prototype thiol-disulfide substitution reactions shown are chosen for their varying electronic and steric effects on the substitution mechanism. Reactions 1 and 2 compare the effect of methyl substitution on the nucleophile, while reactions 1 and 3 compare the steric effect of substitution of the hydrogen on the sulfur under attack with a methyl group. All computations were performed using the GAUSSIAN-98 package.[25]

Our previous computations of reactions 1−3 have shown that the potential energy surfaces obtained with various DFT methods and MP2 and MP4 are consistent.[15] Therefore, B3LYP/6-31+G*[26] computations were performed to determine the lowest energy pathway for reactions 1−3 at each microsolvation level (one to four explicit water molecules) via consideration of the most probable solvation structures for each reactant, product, transition state, and intermediate. Furthermore, although all prior gas-phase studies and the initial solution-phase study have indicated that the reactions proceed via a more favorable trans pathway,[12,13,15] we now reconsider this preference for our more realistic solvation model. Hence, both cis and trans pathways for all three reactions are computed and compared. Analytical frequencies were computed for all B3LYP/6-31+G* optimum geometries to fully characterize the stationary points as well as to obtain the zero-point energies (ZPEs). B3LYP/6-31+G* energies were then corrected for ZPEs scaled by a factor of 0.96.[27]

Following this, B3LYP/6-31+G* single-point free energy computations including PCM[21,28,29] (B3LYP/6-31+G* + PCM) as implemented in GAUSSIAN-98 were performed employing the optimum B3LYP/6-31+G* reaction path microsolvated geometries. Within the PCM model, solvation is modeled as an infinite polarizable continuum (the solvent) surrounding a molecular-shaped cavity (the solute). PCM produces the sum of the electronic energy of the solute and the Gibbs free energy of the continuum solvent. Our hypothesis is as follows: optimization at B3LYP/6-31+G* of the substrate with explicit inclusion of a small number of coordinating water molecules will account for the effects of the first and more important solvation shell (particularly with respect to structure); embedding this optimum microsolvated structure within a polarizable continuum (the PCM method) and performing single-point energy calculations should account for the less important outer solvation shell effects. With this method we hope to gain a more accurate picture of solvation effects in reactions 1−3.

The default uniform dielectric constant of 78.39 for water is used in all calculations. Since our previous attempt to model solvation using the GAUSSIAN-98 default PCM parameters provided nonsensical results, such as transition states lower in energy than the intermediates, we adopt the approach of assigning cavity sizes based on the Mulliken charges at the optimum B3LYP/6-31+G* gas-phase geometries and using eq 1, proposed by Barone et al. for ions.[30]

$$R(\mathrm{X}) = R^0(\mathrm{X}) + \alpha_q|q| \qquad \text{(eq 1)}$$

The atomic radius of each heavy-atom sphere (R(X) where X is the atom) from which the molecular solute cavity is built depends on the atomic radius for the neutral species (R^0(X)) and the charge q, in our case the atomic Mulliken charge. As we did before,[15] the value of α of −0.3 or −0.55 is used for all atoms bearing negative or positive Mulliken charge, respectively.

Results and Discussion

Microsolvation of Reactants. The B3LYP/6-31+G* optimized geometries of thiolate (**1**−**4**), methyl thiolate (**5**−**8**), hydrogen disulfide (**9**−**12**), and methyl hydrodisulfide (**13**−**16**) with one to four water molecules are sketched in Figures 2−5. The microsolvation energies, defined as the energy for the reaction $X + n\ H_2O \rightarrow X(H_2O)_n$ where X = HS^-, MeS^-, HSSH, or MeSSH, are listed in Table 1.

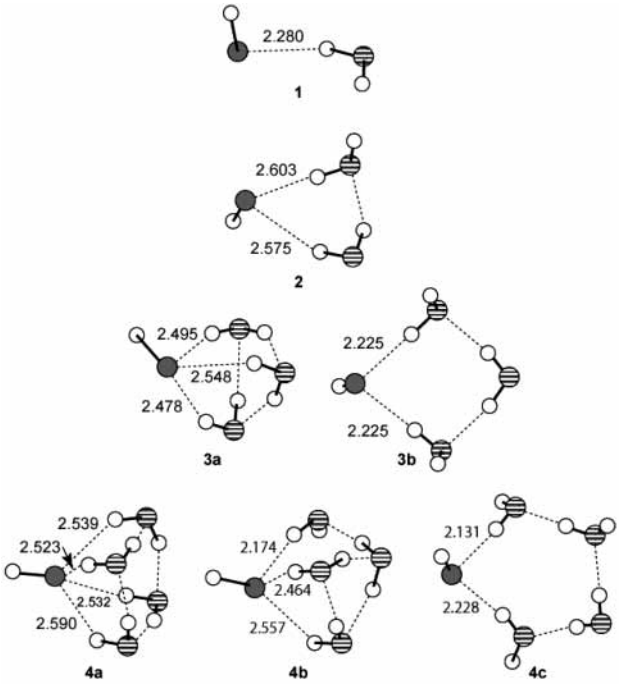

Figure 2. Optimized B3LYP/6-31+G* structures of HS^- with one to four water molecules. Sulfur is indicated by a darkened circle, oxygen by a striped circle, and hydrogen by an empty circle.

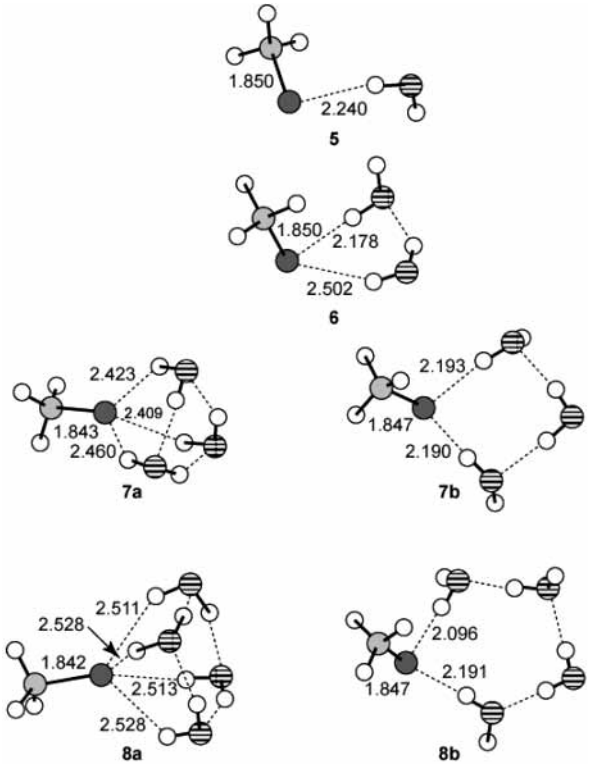

Figure 3. Optimized B3LYP/6-31+G* structures of MeS^- with one to four water molecules. Carbon is indicated by a gray circle, sulfur by a darkened circle, oxygen by a striped circle, and hydrogen by an empty circle.

The water clusters of thiolate and methylthiolate have been examined at the MP2/6-31++G(2d,2p) level and similar levels

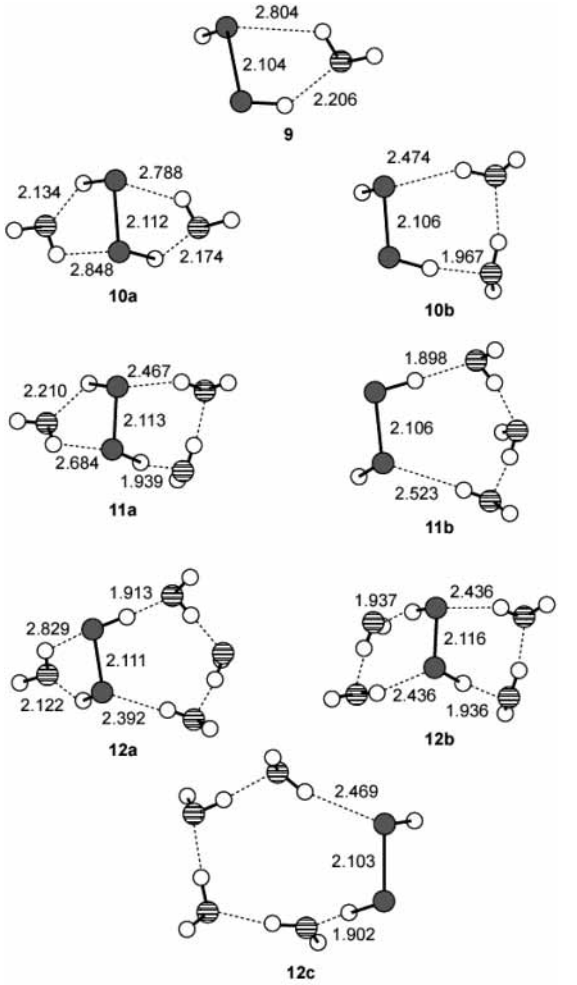

Figure 4. Optimized B3LYP/6-31+G* structures of HSSH with one to four water molecules. See Figure 2 for labels.

TABLE 1: Microsolvation Energy (kcal mol^{-1}) for 1−16

compd	ΔE	compd	ΔE	compd	ΔE	compd	ΔE
1	−13.78	**5**	−14.46	**9**	−2.35	**13**	−2.69
2	−26.53	**6**	−27.34	**10a**	−5.00	**14**	−10.09
				10b	−9.60		
3a	−36.94	**7a**	−37.89	**11a**	−12.65	**15a**	−12.49
3b	−38.81	**7b**	−40.34	**11b**	−16.01	**15b**	−17.78
4a	−49.76	**8a**	−51.18	**12a**	−20.22	**16a**	−20.21
4b	−48.79	**8b**	−50.22	**12b**	−20.50	**16b**	−18.29
4c	−48.50			**12c**	−24.58	**16c**	−25.01

by Masamura.[31,32] They examined a few configurations of clusters containing three to five water molecules, finding the lowest energy form to possess C_3 and C_4 symmetry for the cases where the number of water molecules is 3 or 4, respectively.

Our B3LYP/6-31+G* structures for solvated HS^- and MeS^- are shown in Figures 2 and 3. Only one structure could be found for mono- and disolvated HS^- and MeS^-, even with exhaustive searching for structures with a hydrogen bond where HS^- is the donor. For the trisolvated clusters, the ring structure, which Masamura[31,32] did not examine, is preferred (**3b** and **7b**) due presumably to better hydrogen bonding between the water molecules because of their more linear arrangement about the bridging hydrogen atoms, even though there is one fewer interaction of this type. Of the tetrasolvated clusters, the two with near-C_4 symmetry of the water molecules (**4a** and **8a**) are the lowest in energy, consistent with Masamura's[31,32] results. Furthermore, these microsolvated structures are comparable to the structures of microsolvated fluoride[33] and chloride[24,34,35] anions obtained at HF, MP2, and B3LYP.

The optimized microsolvated structures of HSSH and HSSMe are drawn in Figures 4 and 5. We located one monosolvated structure for each compound (**9** and **13**). The water in each accepts a hydrogen from a sulfur and donates a hydrogen to the adjacent sulfur. There are two structures of disolvated HSSH. The more stable structure, **10b**, has a hydrogen bond between the two waters, which presumably is what leads to its greater stability over **10a**. The only structure for disolvated MeSSH has the waters in similar arrangements as in **10b**. The analogous structure to **10a** is not possible since there is only one donor hydrogen in MeSSH as opposed to two in HSSH. The best trisolvated structure for both HSSH (**11b**) and MeSSH (**15b**) has the three water molecules forming a ring with the disulfide, one water accepting a hydrogen from a sulfur and the third water in the ring donating a hydrogen to the other sulfur. The two strong water−water hydrogen bonds in these structures result in their stability relative to the other configurations, which have a single water−water hydrogen bond. We located three structures for tetrasolvated HSSH and MeSSH, having two, three, or four water molecules in a ring with the disulfide. The lowest energy configurations (**12c** and **16c**) have the four water molecules in a ring, which maximizes the number of water−water hydrogen bonds.

There are two important trends in the microsolvation energies, listed in Table 1. First, unsurprisingly, the anions will associate more strongly with water than the neutral species. A sulfur anion serves as an excellent acceptor in a hydrogen bond. The solvation energies of **1** and **5** provide an estimate of the $S^-\cdots H-O$ hydrogen bond: about 14 kcal mol^{-1}. Further solvation tends to maximize the number of hydrogen atoms donated to the anionic sulfur atom. On the other hand, neutral sulfur only weakly interacts with water; the solvation energy of **9** and **13** is only around 2.5 kcal mol^{-1}. Further solvation will maximize the number of water−water hydrogen bonds.

The second trend is in the association energy with each addition of a water molecule. In the association of water with chloride, the first three water molecules bond with nearly constant strength (about 14−15 kcal mol^{-1}), but the fourth water is more weakly bound (about 12 kcal mol^{-1}).[24,34] For the association of MeS^- with water, experiment has indicated a steady decrease in the association energy with added water molecules, from 15 0.0 kcal mol^{-1} for the first to 9.6 kcal mol^{-1} for the fourth.[36] An MP2/6-31++G(2d,2p) study gave association energies for the first three water molecules in close agreement with experiment.[31] Sieck and Moet-Ner also examined the association of water with HS^-, finding again a steady decrease in the association energy with each added water.[36]

Our calculations for the association of water with HS^- and MeS^- show similar trends of diminishing value with each added water molecule. The association energy of the first water with either anion is 14 kcal mol^{-1}, which compares well with the experimental[36] values (14.2 and 15.0 kcal mol^{-1} for HS^- and MeS^-, respectively). Subsequent water molecules associate with lesser energy; the last water molecules are bound by 11 kcal mol^{-1} to either anion.

Microsolvation Configuration on the Reaction Path. The next question to address is how many explicit water molecules need be incorporated into the computation of the critical points along the reaction pathway. Assuming the addition−elimination mechanism operates here, we focus on the geometries and energetics of the entering transition state and the intermediate. We have not searched for any ion−dipole complexes and

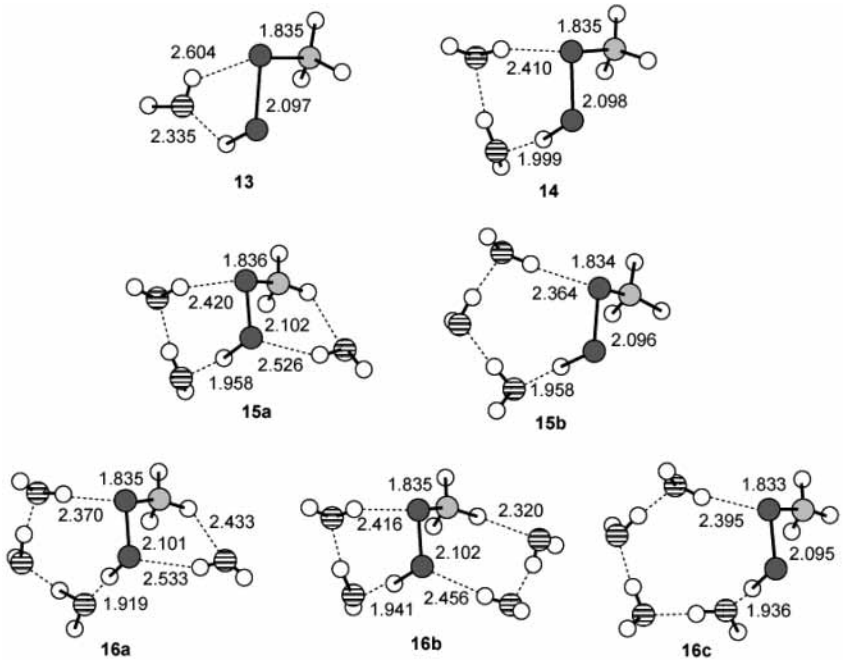

Figure 5. Optimized B3LYP/6-31+G* structures of MeSSH with one to four water molecules. See Figure 3 for labels.

assume their existence in these microsolvated gas-phase reactions. We have employed one to four explicit water molecules solvating these critical points. Important geometric parameters of the entering TS and intermediate for reactions 1−3 with zero to four solvating water molecules are listed in Table 2.

For the unsolvated cases, the intermediates are quite symmetric with regard to the S−S distances. This is distinctly not the case when one to three water molecules are incorporated. For the intermediate of reactions 1 and 2, the difference in the length of the two S−S distances is about 0.3 Å whether one, two, or three water molecules are present. The difference is even larger for reaction 3, as large at 0.77 Å when two water molecules are used. Symmetric structures are again obtained for all three reactions when four water molecules are present, for both the cis and trans pathways.

The geometries of the TSs for reactions 1−3 are less sensitive to the level of solvation. The $S_{nuc}-S$ distance varies by only 0.1 Å for reactions 1 and 2 with differing solvation, while the $S-S_{lg}$ distance decreases systematically with increasing number of water molecules, but here by an overall range of only 0.04 Å. The $S_{nuc}-S$ range is a bit larger for reaction 3, and the $S-S_{lg}$ is little changed by the degree of solvation.

However, examination of the motion of the atoms in the imaginary vibration for the TSs when one, two, or three water molecules are included reveals a significant component due to motion of the waters themselves. This suggests that the transition states are not dominated by the formation of the S−S bond, but rather are related to motions of the waters. Even more worrisome is that since the intermediates are so unsymmetric, there must be at least two intermediates on the pathway, an entrance-like and an exit-like intermediate, and that these must be connected by at least one intervening TS.

Further, on moving from the entrance-like to exit-like intermediate, the water molecules must move greatly, perhaps dominating the overall atomic motions. This is demonstrated in Figure 6, which shows the four critical points along the PES for reaction 1 with two water molecules. **17a** is the entrance transition state, which leads to the intermediate **17b**, 2.8 kcal mol^{-1} below this first TS. This intermediate is quite unsymmetrical, with both water molecules bridging only the nucleophilic sulfur and the sulfur under attack. We next extensively searched for other transition states and intermediates. We found only two more structures, another TS, **17c**, and another intermediate **17d**. The two structures indicate how the two waters move from the nucleophile toward the leaving group. The surface is relatively flat in this region; **17c** and **17d** are 0.35 and 0.29 kcal mol^{-1}, respectively, above **17b**. Since these four points trace only the entrance channel, these four points are duplicated in the exit channel, so the PES is really quite full of small wiggles corresponding largely to the waters migrating across the trisulfide substrate.

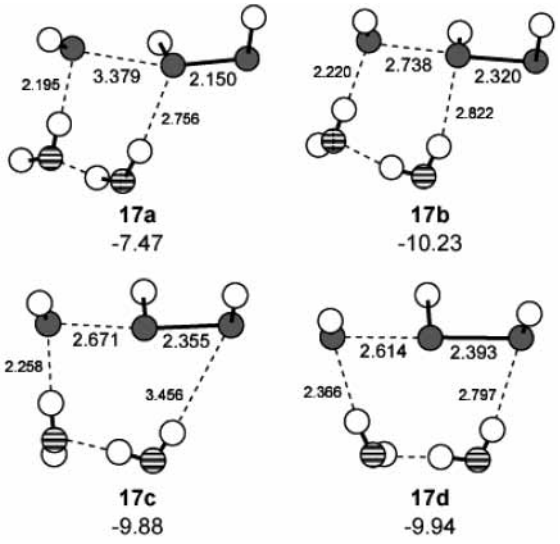

Figure 6. Optimized B3LYP/6-31+G* structures of the four critical points along the PES for reaction 1 with two water molecules. Relative energies (kcal mol^{-1}) are listed below each structure. See Figure 2 for labels.

The PES is simpler and smoother when four water molecules are used to microsolvate the sulfur compounds. The intermediates for all three reactions show the expected near-symmetrical S−S distances. More importantly, the four water molecules can smoothly migrate from near the nucleophile to near the leaving group. Therefore, we will continue the discussion by focusing

TABLE 2: Selected B3LYP/6-31+G* Geometric Parameters for the Cis and Trans (in parentheses) Entering TSs and Intermediates of Reactions 1−3 with Different Levels of Water Solvation

compound	solvation level	$S_{nuc}-S^a$	$S-S_{lg}{}^a$	$RS_{nuc}\cdots H^a$	$S_{nuc}-S-S_{lg}{}^a$
TS-1	0 H_2O^b	(3.238)	(2.185)	(2.427)	(146.0)
	0 H_2O/PCM^{b,c}	(3.311)	(2.121)	(2.467)	(141.8)
	1 H_2O	3.299 (3.294)	2.164 (2.165)	2.489 (2.494)	145.8 (146.1)
	2 H_2O	3.379 (3.396)	2.150 (2.149)	2.601 (2.725)	146.0 (148.7)
	3 H_2O	3.293 (3.283)	2.144 (2.144)	2.529 (2.582)	145.4 (146.8)
	4 H_2O	3.335 (3.336)	2.143 (2.142)	2.602 (2.626)	147.7 (148.2)
INT-1	0 H_2O^b	(2.512)	(2.510)		(173.5)
	0 H_2O/PCM^{b,c}	(2.496)	(2.464)		(175.9)
	1 H_2O	2.641 (2.651)	2.393 (2.388)		173.1 (173.0)
	2 H_2O	2.738 (2.752)	2.320 (2.312)		171.4 (171.7)
	3 H_2O	2.665 (2.692)	2.361 (2.342)		174.4 (174.6)
	4 H_2O	2.503 (2.502)	2.498 (2.500)		174.9 (175.0)
TS-2	0 H_2O^c	(3.173)	(2.177)	(2.432)	(149.1)
	0 H_2O/PCM^{b,c}	(3.298)	(2.120)	(2.454)	(145.9)
	1 H_2O	3.232 (3.232)	2.157 (2.157)	2.506 (2.498)	149.1 (149.2)
	2 H_2O	3.289 (3.318)	2.145 (2.142)	2.531 (2.565)	148.4 (148.0)
	3 H_2O	3.243 (3.250)	2.140 (2.139)	2.600 (2.664)	151.1 (151.6)
	4 H_2O	3.284 (3.287)	2.136 (2.137)	2.637 (2.665)	151.8 (152.4)
INT-2	0 H_2O^c	(2.498)	(2.496)		(173.9)
	0 H_2O/PCM^{b,c}	(2.477)	(2.463)		(175.5)
	1 H_2O	2.655 (2.663)	2.355 (2.352)		173.3 (176.4)
	2 H_2O	2.748 (2.776)	2.289 (2.278)		171.7 (172.5)
	3 H_2O	2.671 (2.645)	2.337 (2.358)		174.7 (174.9)
	4 H_2O	2.503 (2.496)	2.470 (2.484)		176.4 (175.4)
TS-3	0 H_2O^c	(4.004)	(2.114)	(2.580)	(166.9)
	0 H_2O/PCM^{b-d}				
	1 H_2O	3.952 (3.932)	2.121 (2.122)	2.626 (2.624)	169.1 (169.2)
	2 H_2O	3.969 (3.888)	2.116 (2.117)	2.647 (2.678)	168.7 (162.8)
	3 H_2O	3.588 (3.420)	2.120 (2.130)	2.688 (2.755)	168.0 (166.0)
	4 H_2O	3.748 (3.581)	2.116 (2.125)	2.748 (2.820)	170.7 (169.5)
INT-3	0 H_2O^c	(2.562)	(2.491)		(175.3)
	0 H_2O/PCM^{b-d}	(2.524)	(2.470)		(174.4)
	1 H_2O	2.785 (2.801)	2.326 (2.318)		176.1 (176.4)
	2 H_2O	3.001 (2.973)	2.229 (2.234)		177.0 (176.7)
	3 H_2O	2.857 (2.932)	2.282 (2.247)		174.8 (174.7)
	4 H_2O	2.531 (2.544)	2.500 (2.495)		175.8 (175.9)

[a] S_{nuc} = nucleophilic sulfur; S_{lg} = leaving sulfur; S = sulfur under attack; distances are in Å and angles in deg. [b] From ref 15. [c] B3LYP/6-31+G* + PCM. [d] **INT-3** is actually a transition state at B3LYP/6-31+G* + PCM.

on the tetrasolvated reactions only. It must be pointed out that further addition of solvating water molecules may alter the geometries and energetics. However, the strongest interaction between the solvent and the substrate will be in the region near the anionic portion of the substrate. The four water molecules we have used are placed near this region. Any additional water molecules will interact with the substrate or these first four molecules via normal hydrogen bonding, which should be adequately described by PCM. In other words, water molecules that interact on the other side of the substrate are likely to be adequately accounted for in PCM.

The next consideration is the configurations of the four water molecules. One can imagine a myriad of configurations of four water molecules about the substrate. For the reactions examined here, the configurations are dictated by a balance of hydrogen bonding between the water molecules and hydrogen bonding between water and sulfur of the substrate. We located a number of structures of the intermediate of reaction 1, differing principally in their water configuration. In Figure 7 we present a number of these configurations that are all intermediates in terms of the substitution reaction, i.e., a stable trisulfide, and all have only real frequencies. Below each structure we list their relative energy at B3LYP/6-31+G* with ZPE correction and the PCM energy using this B3LYP optimized geometry.

The top two structures, **18a** and **18b**, have the four water molecules as a cluster, containing four hydrogen bonds among themselves. The cis isomer is slightly lower in energy (both with and without inclusion of PCM for treatment of the bulk solution) than the trans isomer and is the lowest energy structure we located. The next two, **18c** and **18d**, were attempts to locate structures having the four water molecules isolated from each other, successfully found in the trans case, but we could only locate **18c** for the cis case. The last four structures represent configurations with two water dimers associated with opposite ends of the trisulfide substrate. All of these alternative configurations are 8−11 kcal mol^{-1} higher in energy than the water cluster configurations (**18a** and **18b**), even in the PCM model. Mohamed and Jensen[24] opted for the extended configurations, like **18e**,**f**, in their study of S_N2 reactions, arguing that these extended structures would more favorably interact with the bulk solvent than would the closed cluster. However, we find the opposite: the closed cluster is lower in energy than the extend configurations at B3LYP/6-31+G* + PCM. The closed cluster maintains optimum hydrogen bonding both within the collection of water molecules and with the substrate, along with favorable interaction with the bulk. Given this strong energetic preference for the cluster and that it allows for smooth movement of the waters from nucleophile to leaving group along the reaction path, we have opted to examine reactions 1−3 using only this type of configuration. Nonetheless, we offer the disclaimer that these results represent a qualitative representation of the microsolvated potential energy surface and that one should be cautious to not overemphasize the relative energies of the critical points. However, the topological features, particularly the presence (addition−elimination) or absence (S_N2) of intermediates, will discern the reaction mechanism.

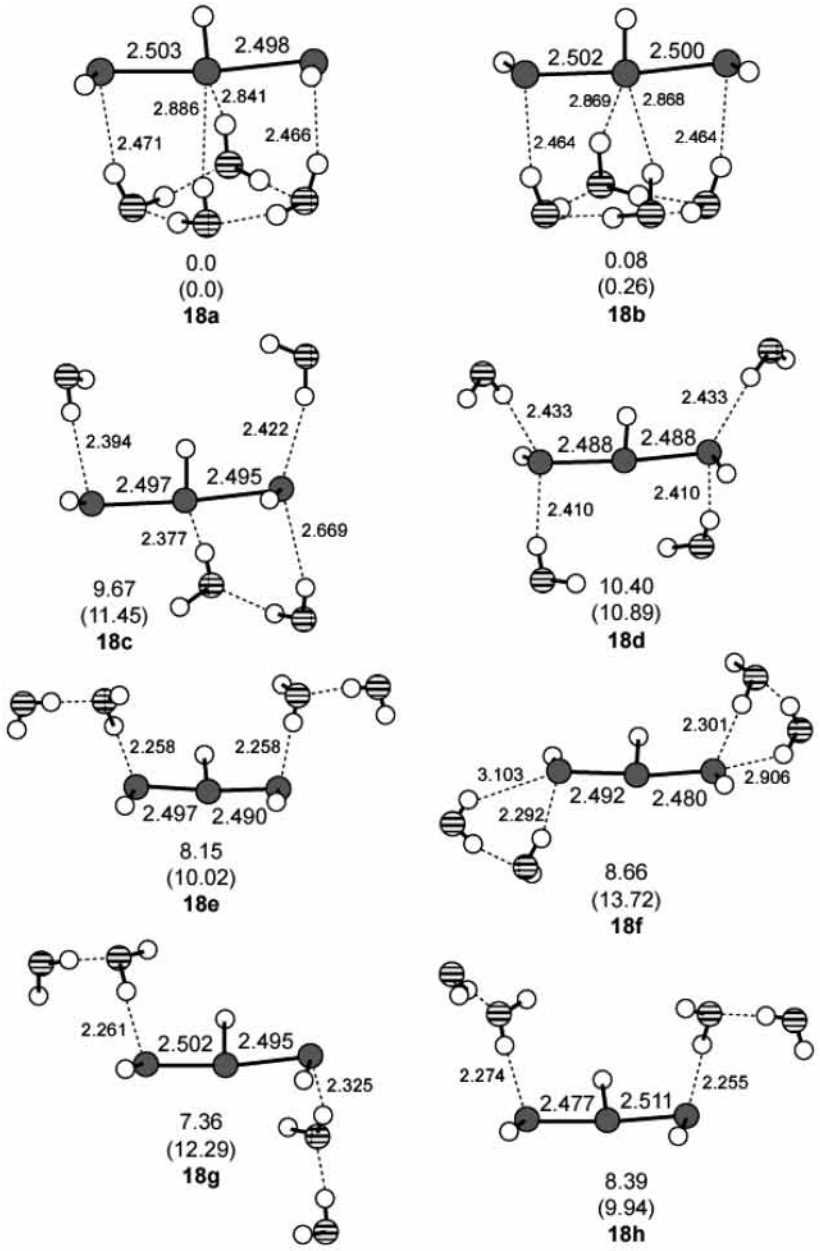

Figure 7. Optimized B3LYP/6-31+G* structures of the intermediate of reaction 1 with differing water configurations. Below each structure is its relative energy at B3LYP/6-31+G* and, in parentheses, at B3LYP/6-31+G* + PCM. See Figure 2 for labels.

Microsolvated Potential Energy Surfaces for Reactions 1−3. The discussion continues with the important geometric features and energetics of reactions 1−3 with four water molecules arranged as a cluster. Important geometric data are listed in Table 2, and the structures at the critical points are drawn in Figures 8−10. To place these results in proper context, the results of our previous PCM optimizations[15] without explicit solvation are presented in Table 2 as "0 H_2O/PCM".

Reactions 1 and 2 represent nucleophilic substitution at a sulfur atom that bears a hydrogen atom. The dominant atomic motion in the first transition state is the cleavage of the hydrogen bond between the nucleophile and the hydrogen on sulfur (the $RS_{nuc}\cdots H$ distance) and formation of the $S_{nuc}-S$ bond. Analysis of Table 2 reveals four main points with respect to the first transition states for these two reactions. (a) The gross structures of **TS-1** and **TS-2** are quite similar, for both the gas phase and solution. (b) Solvation leads to earlier entering transition states for both reactions; the $S_{nuc}-S$ distance is 0.1 Å longer and the $S-S_{lg}$ distance is 0.04 Å shorter in the microsolvated TSs than for the gas phase. (c) There is little geometric difference between the cis and trans TSs. (4) The PCM and microsolvated TSs are very similar in structure; the sole significant difference is the longer $RS_{nuc}\cdots H$ distance in the microsolvated geometries.

The intermediates of reactions 1 and 2, **INT-1** and **INT-2**, are also similar, and the key geometric parameters are insensitive to whether the approach is cis or trans. Furthermore, the geometries of these intermediates are extremely similar whether optimized in the gas phase, with microsolvation by four water molecules, or with PCM; the S−S distances differ by less than 0.04 Å.

The energetics of reactions 1 and 2 with four water molecules are presented in Table 3. (The energetics for these reactions with one to three water molecules are listed in Table S1.) The qualitative potential energy surfaces for these reactions are drawn in Figure 11. We have not located the ion−dipole complexes and draw their well as a dashed line to indicate their presence without any knowledge of the well depth.

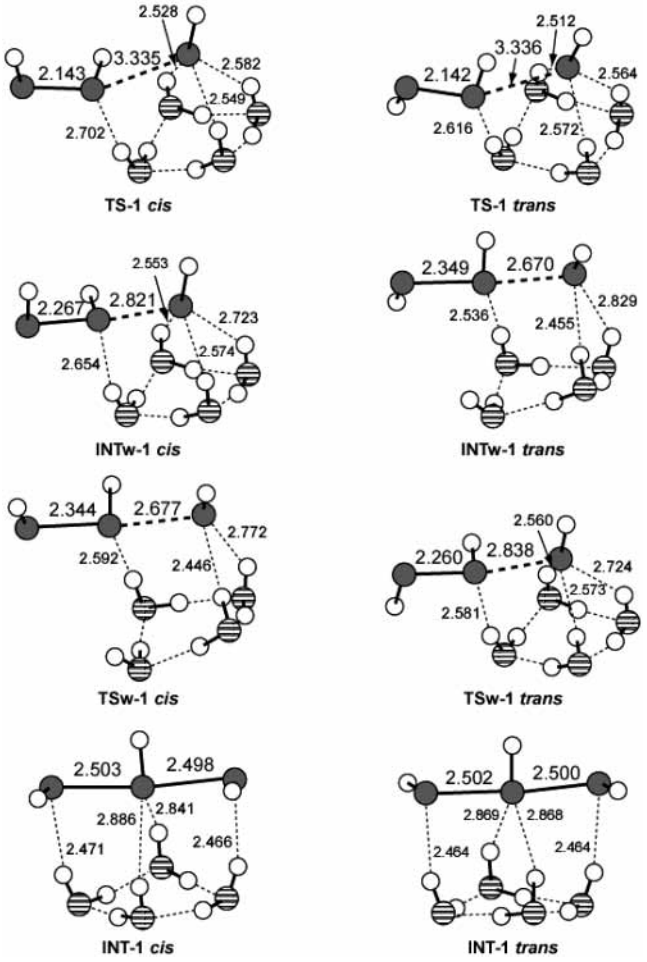

Figure 8. Optimized B3LYP/6-31+G* structures of the microsolvated critical points of reaction 1. See Figure 2 for labels.

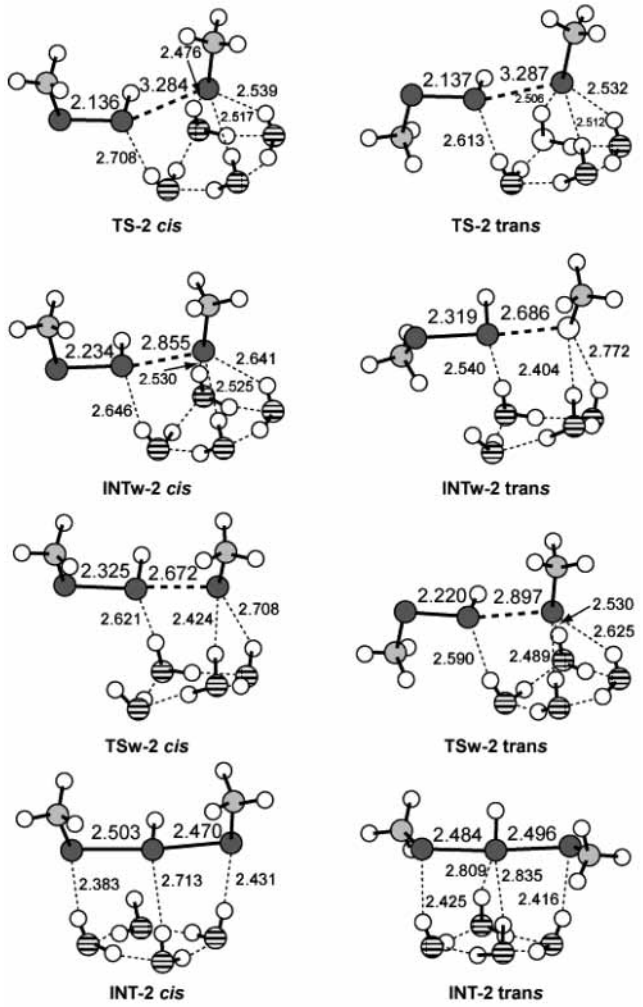

Figure 9. Optimized B3LYP/6-31+G* structures of the microsolvated critical points of reaction 2. See Figure 3 for labels.

The qualitative shapes of the PESs change dramatically upon solvation. The gas-phase surface has three wells, as shown in Figure 1a. The microsolvated surface has another TS (**TSw**) and intermediate (**INTw**) corresponding principally to motion of the water cluster (see Figure 11a,b). As an aside, it is worth noting that the transition states and intermediates associated with motion of the water cluster may be an artifact due to the limited number of explicit water molecules employed in our model. The cis and trans pathways are topologically identical, with minimal energetic differences; the largest difference is that the trans entering transition states are slightly more favorable than the cis TSs.

The presence of an intermediate on the reaction surface is the critical feature in determining the mechanism, principally in rejecting the S_N2 mechanism. The significance of the intermediate is dependent on the depth of its well. For the gas phase, the well depth, evaluated as the energy difference between the TS and intermediate, is 5.1 and 4.2 kcal mol^{-1} for reactions 1 and 2, respectively. For the microsolvated surfaces, we define the well depth as the energy difference between the intermediate and the highest TS (**TS-1** for reaction 1 and **TSw-2** for reaction 2). With the four water molecules, the well depth decreases to 2.8 kcal mol^{-1} (2.4 for the trans path) for reaction 1 and 1.8 kcal mol^{-1} (2.2 for the trans path) for reaction 2. These well depths can be compared to those computed for the trans pathway at B3LYP with PCM:[15] 3.3 and 2.3 kcal mol^{-1} for reactions 1 and 2, respectively. Last, all of our computations (gas phase with a variety of post-HF methods, solution phase by PCM or microsolvation) indicate that reactions 1 and 2 proceed by the addition−elimination method.

Reaction 3 examines nucleophilic substitution at a sulfur atom that bears a methyl group. Unlike for reactions 1 and 2, microsolvation leads to a later initial TS. In **TS-3**, the $S_{nuc}-S$ distance is 4.004 Å for the gas phase, but shrinks to 3.748 Å for the tetrasolvated cis path and is even shorter (3.581 Å) for the tetrasolvated trans path. This also represents the largest geometric difference between any of the cis and trans critical points for reaction 3. Both the gas-phase and microsolvated TSs are much earlier than in reactions 1 and 2, due to the weaker hydrogen bond between thiolate and the methyl hydrogen versus between thiolate and the hydrogen on sulfur. The larger steric inhibition imposed by the methyl group versus a hydrogen is also a factor. Interestingly, no entrance TS for reaction 3 was located at B3LYP with PCM.[15] Rather, in this case, an S_N2 mechanism was observed having a symmetric TS, similar in geometry to the intermediates located here.

The microsolvated intermediates for reaction 3 on both the cis and trans pathways are quite symmetric (the two S−S distances differ by less than 0.01 Å). They are also quite similar to the gas-phase intermediate and to each other.

The relative energies for the critical points of microsolvated reaction 3 are listed in Table 3, and a sketch of the PES is drawn in Figure 11c. The overall shapes of the cis and trans PESs are identical, although the relative energies do differ. The trans entrance TS (**TS-3**) is lower than the cis. The first intermediate

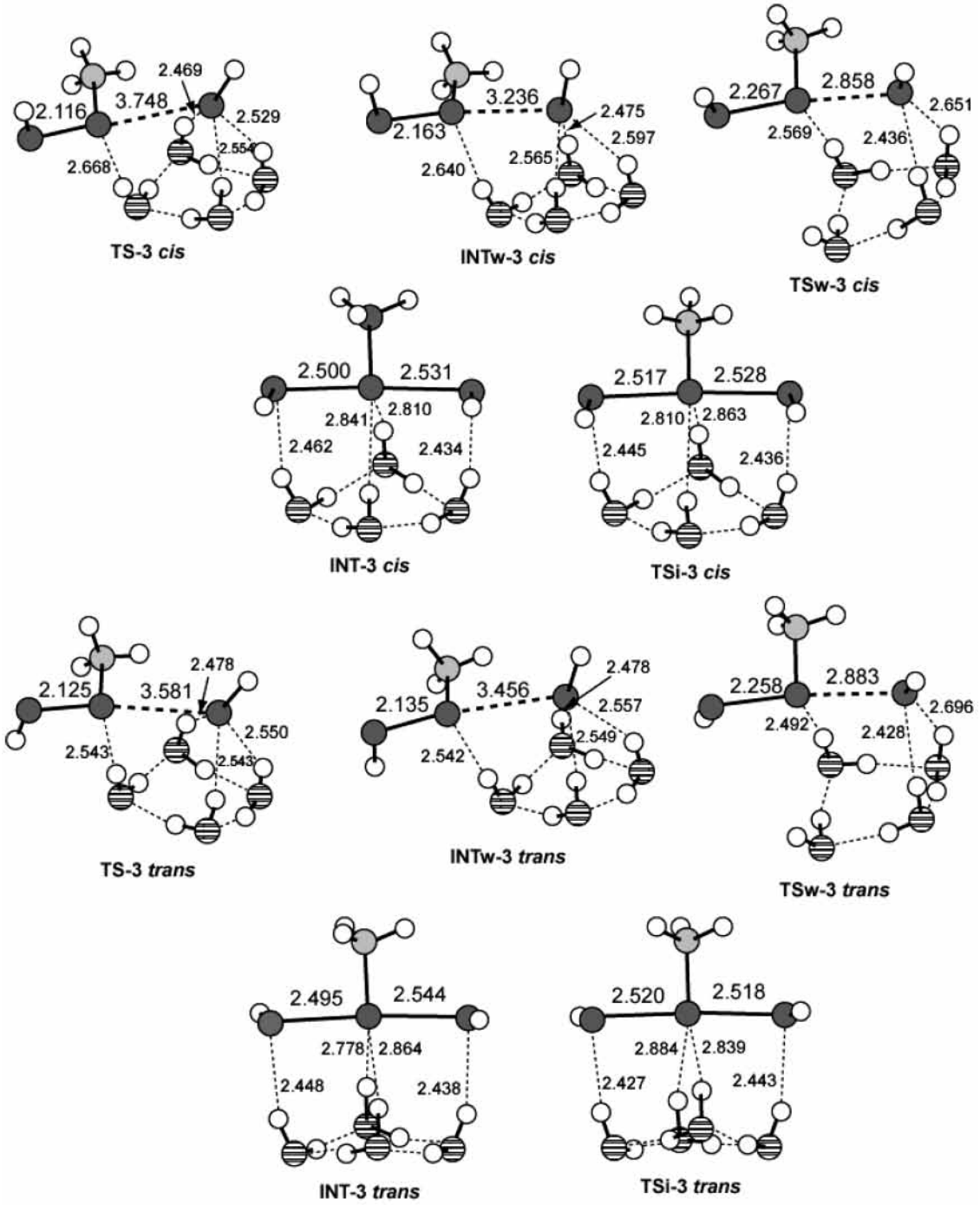

Figure 10. Optimized B3LYP/6-31+G* structures of the microsolvated critical points of reaction 3. See Figure 3 for labels.

TABLE 3: Relative Energies (kcal mol^{-1}) at B3LYP/6-31+G* of the Cis and Trans (in parantheses) Pathways for Reactions 1−3 Including Four Water Molecules

reactants	TS	INTw	TSw	INT	TSi
		Reaction 1			
9.95	2.79 (2.48)	1.69 (1.45)	2.23 (2.09)	0.0 (0.09)	
		Reaction 2			
7.93	1.77 (1.32)	1.19 (0.89)	2.13 (2.19)	0.33 (0.0)	
		Reaction 3			
4.53	0.38 (−0.08)	0.29 (−0.07)	1.44 (1.33)	0.0 (0.29)	0.55 (0.22)

is just below the energy of **TS-3**. (Location of **INTw-3** on the trans pathway is quite difficult. The surface is very flat, and the structure we located is nearly identical in energy to **TS-3**, although it does have only real frequencies.) The next TS, which corresponds largely to movement of the water cluster across the substrate, is actually the highest barrier on both the cis and trans surfaces. (Again, we note that critical points associated with water cluster motion may be artifacts of the limited number of water molecules included in the model.) Next comes the intermediate **INT-3**. For the cis path, **INT-3** is the lowest energy critical point, lying 4.51 kcal mol^{-1} below reactants. For the trans path, **INT-3** lies above **INTw-3**. The cis intermediate is 0.3 kcal mol^{-1} more stable than the trans intermediate. The entrance and exit channels are connected by a transition state corresponding principally to rotation of the methyl group (**TSi-3**). The height of this barrier is about 0.5 kcal mol^{-1} on the *cis* path. **TSi-3** actually lies below **INT-3** on the trans path when ZPE is included.

The highest barrier for reaction 3 corresponds to **TSw-3**. The difference in energy of **INT-3** and this highest barrier gives the

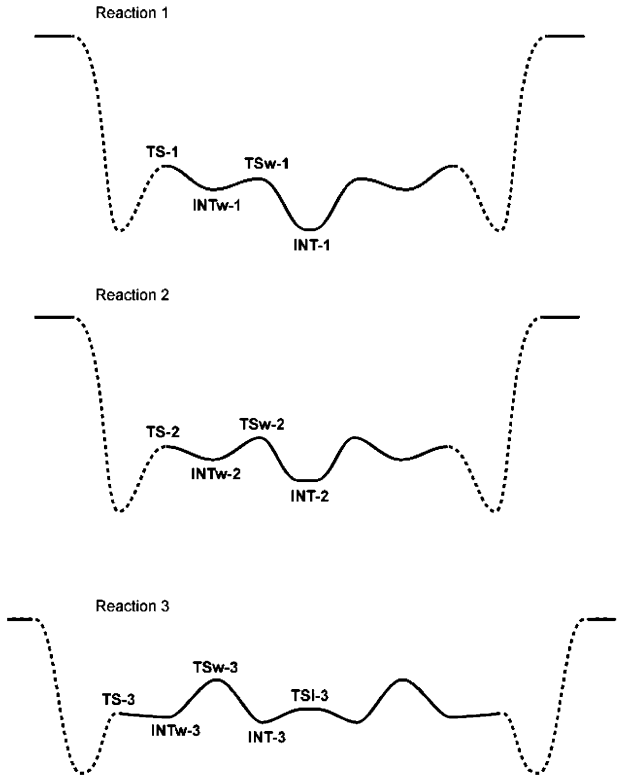

Figure 11. Qualitative microsolvated potential energy surfaces for reactions 1−3 at B3LYP/6-31+G*.

TABLE 4: Relative Energies (kcal mol^{-1}) at B3LYP/6-31+G* + PCM of the Cis and Trans (in parantheses) Pathways for Reactions 1−3 Including Four Water Molecules

TS	INTw	TSw	INT	TSi
		Reaction 1		
2.87 (2.69)	1.93 (2.23)	0.97 (2.03)	0.0 (0.0)	
		Reaction 2		
3.31 (1.10)	2.91 (1.85)	3.32 (2.40)	0.0 (0.0)	
		Reaction 3		
−1.90 (−1.44)	−1.11 (−1.51)	−1.10 (−1.53)	0.0 (0.0)	−0.04 (−0.16)

well depth: 1.4 kcal mol^{-1} for the cis path and 1.0 kcal mol^{-1} for the trans path. These barriers are very small. Nevertheless, the addition−elimination mechanism operates for reaction 3 with microsolvation.

Microsolvation with PCM. To account for long-range solvation effects, we performed B3LYP/6-31+G* including PCM (B3LYP/6-31+G* + PCM) single-point energy calculations on each of the B3LYP/6-31+G* optimized microsolvated geometries for each pathway. It is worth reiterating that it was necessary to alter the atomic radii of the heavy atoms defining the cavity to properly account for the varying charge distributions in the transition states and intermediates. The purpose of these single-point computations is to model bulk solvation to determine its effect on the mechanism. Since the geometries are not reoptimized at this level, due to size restrictions and optimization instabilities, we emphasize only the qualitative relative energies of the critical points. These relative energies for reactions 1−3 are listed in Table 4.

For reaction 1, the relative energies of the critical points decrease monotonically from **TS-1** to **INT-1**. This is the case for both the cis and trans pathways, although **TS-1** is higher on the cis path, but the energy drops less rapidly on the trans surface. These surfaces possess an intermediate with a barrier entering and exiting this intermediate.

For the trans path of reaction 2, we see increasing energy from **TS-2** to **TSw-2** and the lowest energy critical point is the intermediate. This surface too possesses an intermediate with a barrier entering and exiting the intermediate. The cis path has different behavior; the energy decreases from **TS-2** to **INTw-2**, then rises to **TSw-2** and then falls into a much deeper well at **INT-2**. This surface is thus topologically unchanged from that found without PCM.

Reactions 1 and 2 continue to have at least one intermediate on the reaction path with the incorporation of both microsolvation and PCM. The potential energy surfaces of reaction 1 and the trans path of reaction 2 appear to be that of a simple addition−elimination reaction. The cis path of reaction 2 retains the extra well observed upon addition of the water cluster, yet remains an addition−elimination mechanism. Our previous study[15] where we optimized the structures at B3LYP including PCM also indicated an addition−elimination mechanism.

Incorporation of the bulk solvent using PCM substantively alters the PES of reaction 3. Now **INT-3** is the highest energy critical point, with the energies increasing steadily from **TS-3** to **INT-3**. Instead of one or two intermediates on the surface, incorporation of the bulk solvent suggests that there are no intermediates on the reaction path. (The dip in energy associated with **TSi-3** is too small to be significant, especially since we have not optimized structures nor confirmed their nature with a frequency analysis.) The reaction mechanism is therefore S_N2, with standard backside attack of the nucleophile and a single transition state. This is also in agreement with our previous study using optimized PCM structures.

Conclusions

Previous gas-phase studies of nucleophilic substitution at sulfur indicated that the reaction proceeds via an addition−elimination mechanism.[12,13] Incorporation of the bulk effect of solvent (water) using the polarized continuum method indicated an addition−elimination mechanism when the sulfur under attack has a hydrogen atom attached (reactions 1 and 2), but an S_N2 mechanism when a methyl group is attached (reaction 3).[15] The computations reported here consider local solvent effects by including four water molecules as a cluster to microsolvate the reactants and long-range effects using PCM.

Reactions 1 and 2, having a small substituent (hydrogen) on the sulfur under attack, follow the addition elimination mechanism regardless of level examined: gas-phase, optimized geometries at PCM, microsolvated with four water molecules, and microsolvated with PCM. On the other hand, the mechanism of reaction 3 is sensitive to the computational approach. In the gas phase, the mechanism is addition−elimination, although the well depth of the intermediate is quite shallow. The mechanism remains addition−elimination with microsolvation. However, the mechanism is S_N2 when PCM is used, whether on its own or with the microsolvated structures.

Solvation increases the stability of the transition states relative to the intermediates and hence reduces the depths of wells associated with the intermediates. For reactions 1 and 2, which have sizable wells (4−5 kcal mol^{-1}) for the gas-phase intermediate, the intermediate persists when water is included. For reaction 3, where the well is shallower (3 kcal mol^{-1}), the intermediate disappears and the reaction mechanism switches to S_N2 upon solvation. Substituents that stabilize the intermediate in the gas phase should therefore lead to addition−elimination pathways in solution. Such precise partitioning of the mechanism of these reactions into two separate concepts (S_N2 vs A−E) is perhaps stretching the point since the potential energy surfaces

are flat in the neighborhood of the transitions states and intermediates. Nevertheless, these concepts guide the way physical organic chemists think about these reactions, and this study does indicate the sensitivity of these reactions to phase.

Acknowledgment. We acknowledge financial support for this work from the Robert A. Welch Foundation (W-1442) and the Petroleum Research Fund, administered by the American Chemical Society.

Supporting Information Available: Table S1 and coordinates of all optimized B3LYP/6-31+G* structures, their absolute energies, and number of imaginary frequencies. This material is available free of charge via the Internet at http://pubs.acs.org.

References and Notes

(1) Mathews, C. K.; van Holde, K. E. *Biochemistry*; Benjamin/Cummings: Redwood City, CA, 1990.
(2) Liu, T.-Y. In *The Proteins*; Neurath, H., Hill, R. L., Boeder, C.-L., Eds.; Academic Press: New York, 1977; pp 239−402.
(3) Williams, C. H. J. In *The Enzymes*; Boyer, P. D., Ed.; Academic Press: New York, 1976; Vol. 13, pp 89−173.
(4) Whitesides, G. M.; Lilburn, J. E.; Szajewski, R. P. *J. Org. Chem.* **1977**, *42*, 332.
(5) Wilson, J. M.; Bayer, R. J.; Hupe, D. J. *J. Am. Chem. Soc.* **1977**, *99*, 7922−7926.
(6) Freter, R.; Pohl, E. R.; Hupe, D. J. *J. Org. Chem.* **1979**, *44*, 1771−1774.
(7) Szajewski, R. P.; Whitesides, G. M. *J. Am. Chem. Soc.* **1980**, *102*, 2011.
(8) Whitesides, G. M.; Houk, J.; Patterson, M. A. K. *J. Org. Chem.* **1983**, *48*, 112−115.
(9) Hupe, D. J.; Pohl, E. R. *Isr. J. Chem.* **1985**, *26*, 395−399.
(10) Singh, R.; Whitesides, G. M. *J. Am. Chem. Soc.* **1990**, *112*, 1190−1197.
(11) Singh, R.; Whitesides, G. M. *J. Am. Chem. Soc.* **1990**, *112*, 6304−6309.
(12) Bachrach, S. M.; Mulhearn, D. C. *J. Phys. Chem.* **1996**, *100*, 3535−3540.
(13) Mulhearn, D. C.; Bachrach, S. M. *J. Am. Chem. Soc.* **1996**, *118*, 9415−9421.
(14) Bachrach, S. M.; Gailbreath, B. D. *J. Org. Chem.* **2001**, *66*, 2005−2010.
(15) Bachrach, S. M.; Hayes, J. M.; Dao, T.; Mynar, J. L. *Theor. Chem. Acc.* **2002**, *107*, 266−271.
(16) Gailbreath, B. D.; Pommerening, C. A.; Bachrach, S. M.; Sunderlin, L. S. *J. Phys. Chem. A* **2000**, *104*, 2958−2961.
(17) Bachrach, S. M.; Hayes, J. M.; Check, C. E.; Sunderlin, L. S. *J. Phys. Chem. A* **2001**, *105*, 9595−9597.
(18) Tanaka, K.; Mackay, G. I.; Payzant, J. D.; Bohme, D. K. *Can. J. Chem.* **1976**, *54*, 1643−1659.
(19) Brauman, J. I.; Olmstead, W. N.; Lieder, C. A. *J. Am. Chem. Soc.* **1974**, *96*, 4030−4031.
(20) Chandrasekhar, J.; Smith, S. F.; Jorgenson, W. L. *J. Am. Chem. Soc.* **1984**, *106*, 3049−3050.
(21) Cossi, M.; Barone, V.; Cammi, R.; Tomasi, J. *Chem. Phys. Lett.* **1996**, *255*, 327.
(22) Cossi, M.; Barone, V. *J. Chem. Phys.* **1998**, *1998*, 6246−6254.
(23) Barone, V.; Cossi, M.; Tomasi, J. *J. Comput. Chem.* **1998**, *19*, 404−417.
(24) Mohamed, A. A.; Jensen, F. *J. Phys. Chem. A* **2001**, *105*, 3259−3268.
(25) Frisch, M. J.; Trucks, G. W.; Schlegel, H. B.; Scuseria, G. E.; Robb, M. A.; Cheeseman, J. R.; Zakrzewski, V. G.; Montgomery, J. A. J.; Stratmann, R. E.; Burant, J. C.; Dapprich, S.; Millam, J. M.; Daniels, A. D.; Kudin, K. N.; Strain, M. C.; Farkas, O.; Tomasi, J.; Barone, V.; Cossi, M.; Cammi, R.; Mennucci, B.; Pomelli, C.; Adamo, C.; Clifford, S.; Ochterski, J.; Petersson, G. A.; Ayala, P. Y.; Cui, Q.; Morokuma, K.; Malick, D. K.; Rabuck, A. D.; Raghavachari, K.; Foresman, J. B.; Cioslowski, J.; Ortiz, J. V.; Baboul, A. G.; Stefanov, B. B.; Liu, G.; Liashenko, A.; Piskorz, P.; Komaromi, I.; Gomperts, R.; Martin, R. L.; Fox, D. J.; Keith, T.; Al-Laham, M. A.; Peng, C. Y.; Nanayakkara, A.; Gonzalez, C.; Challacombe, M.; Gill, P. M. W.; Johnson, B.; Chen, W.; Wong, M. W.; Andres, J. L.; Gonzalez, C.; Head-Gordon, M.; Replogle, E. S.; Pople, J. A. *GAUSSIAN-98*, A.7 ed.; Gaussian, Inc.: Pittsburgh, PA, 1998.
(26) Becke, A. D. *J. Chem. Phys.* **1993**, *98*, 5648−5650. (b) Lee, C.; Yang, W.; Parr, R. G. *Phys. Rev. B* **1988**, *37*, 785−789. (c) Vosko, S. H.; Wilk, L.; Nusair, M. *Can. J. Phys.* **1980**, *58*, 1200−1211. (d) Stephens, P. J.; Devlin, F. J.; Chabalowski, C. F.; Frisch, M. J. *J. Phys. Chem.* **1994**, *98*, 11623−11627.
(27) Wong, M. H. *Chem. Phys. Lett.* **1996**, *256*, 391−399.
(28) Miertus, S.; Scrocco, E.; Tomasi, J. *Chem. Phys.* **1981**, *55*, 117−129.
(29) Miertus, S.; Tomasi, J. *Chem. Phys.* **1982**, *65*, 239−245.
(30) Barone, V.; Cossi, M.; Tomasi, J. *J. Chem. Phys.* **1997**, *107*, 3210−3221.
(31) Masamura, M.; Ikuta, S. *J. Comput. Chem.* **1999**, *11*, 1138−1144.
(32) Masamura, M. *Chem. Phys. Lett.* **2001**, *339*, 279−289.
(33) Xantheas, S. S.; Dunning, T. H., Jr. *J. Phys. Chem.* **1994**, *98*, 13489−13497.
(34) Okuno, Y. *J. Chem Phys.* **1996**, *105*, 5817−5829.
(35) Okuno, Y. *J. Am. Chem. Soc.* **2000**, *122*, 2925−2933.
(36) Sieck, L. W.; Moet-Ner (Mautner), M. *J. Phys. Chem.* **1989**, *93*, 1586−1588.